A Spectrally Tunable Smart LED Lighting System With Closed-Loop Control

Ivan Chew, Vineetha Kalavally, *Member, IEEE*, Chee Pin Tan, *Senior Member, IEEE*, and Jussi Parkkinen

***Abstract*— Light emitting diodes (LEDs), with their ability to produce tunable light spectrums, present a significant opportunity to improve on existing lighting systems. They can be applied to smart and specialized lighting, which can be highly beneficial in the residential, commercial, and industrial sectors. In this paper, we present a novel closed-loop control algorithm with feedback from a spectral sensor, which allows the light output spectrum to converge toward a target spectrum. The control system was experimentally validated by the hardware implementation of a wireless smart lighting system with the eight tunable LED channels with different dominant wavelengths (450–650 nm) designed to cover a large portion of the visible light spectrum. Experimental results show a near perfect replication of target spectra, with an accuracy within 5% for the correlated color temperatures and Euclidean distances which fall well within a five-step u′v′ unit circle.**

***Index Terms*— Smart lighting, intelligent lighting, lighting control, spectral sensing, light spectrum control, LEDs.**

I. Introduction

SMART grids are the next step in the evolution of traditional electric power infrastructure, promising more efficient power management and greater reliability. Intelligent devices such as thermostats, smart meters and sensors have recently been integrated into smart grid systems with varying degrees of success. As the world moves towards a more connected future, there is growing demand to bridge the gap between lighting and smart grid systems through smart lighting. Smart lighting evolves from traditional lighting control by utilizing a closed-loop control system with feedback from integrated sensors. Current smart lighting systems also integrate well with existing wireless networks in buildings to offer users remote control over the smart lights [1], [2].

Connectivity forms the backbone of a smart grid solution. The communication network needs to be able to facilitate reliable bi-directional communication between multiple smart grid devices. There are many different connectivity options for smart lighting. For wired solutions, there are the Digital Addressable Lighting Interface (DALI), Digital Multiplex (DMX512), Phillips LightMaster KNX, Ethernet, and Power Line Communications (PLC) interfaces. Wireless lighting networks are often easier to implement compared to wired solutions, which may require extensive cabling. Moreover, wired solutions are often difficult to retrofit for existing buildings. Common wireless protocols include the IEEE 802.15.4 ZigBee standard, the IEEE 802.11a/b/g/n/ac Wi-Fi standard, the IEEE 802.15.1 Bluetooth standard and the Bluetooth LE 4.0 standard. The IEEE 802.15.4 ZigBee standard is often used for low-rate wireless networks due to its low cost, low power consumption and low complexity [3]. Wireless ZigBee networks have been applied to road lighting [4]–[6], office lighting [7], and home lighting [8]–[10]. The wireless network can also connect wireless sensor modules to provide accurate feedback about the immediate environment to the controller [11].

The advent of light emitting diodes (LEDs) greatly benefit smart lighting systems, as they are essentially electronic components with excellent dimming capabilities and very narrow peak bandwidths, which allow a great degree of control over the produced light spectrum. Besides that, LEDs have other attractive properties such as low power consumption, long lifetime, no poisonous mercury content, and an increasing luminous efficacy [12].

Currently, smart lighting systems are generally focused on energy savings [13]–[15] as there is huge potential to reap significant energy savings when smart lighting control is used in conjunction with efficiently driven LEDs [16], [17]. In fact, systems with integrated smart lighting control typically report savings of 17% - 60% over traditional lighting control depending on the occupant usage patterns [18]. Unfortunately, most of these systems exclusively consider energy savings in isolation without addressing other pressing issues such as occupant comfort and light quality. Recently, some researchers have begun considering these factors in addition to increasing the system energy efficiency. For example, Tan et al. proposed the use of smart wireless sensors for personal control of an LED lighting system to cater to individual user preferences while gleaning high energy savings [7]. Similarly, Byun et al. also considered user satisfaction and energy efficiency concurrently by collecting user feedback via wireless devices [19]. More recently, Higuera et al. designed a smart lighting system that is ISO/IEC/IEEE 21451 compatible, achieving up to 43% energy savings while exhibiting an increase in occupant visual comfort [20].

Manuscript received February 18, 2016; revised March 11, 2016; accepted March 11, 2016. Date of publication March 15, 2016; date of current version April 26, 2016. This work was supported by the Collaborative Research in Engineering, Science and Technology through the Project entitled Quality of Light–Impact of Visual and Non-Visual Effects under Grant P20C1-15. The associate editor coordinating the review of this paper and approving it for publication was Prof. Kazuaki Sawada.

I. Chew and V. Kalavally are with the Department of Electrical and Computer Systems Engineering, Monash University Malaysia, Bandar Sunway 47500, Malaysia (e-mail: ivan.chew@monash.edu; vineetha@monash.edu).

C. P. Tan is with the Department of Mechatronics Engineering, Monash University Malaysia, Bandar Sunway 47500, Malaysia (e-mail: tan.chee.pin@monash.edu).

J. Parkkinen is with the School of Computing, University of Eastern Finland, Joensuu 80130, Finland (e-mail: jussi.parkkinen@uef.fi).

Digital Object Identifier 10.1109/JSEN.2016.2542265

Another key area of research in the smart lighting field is the control of the correlated color temperature (CCT). This is important because it has been shown that the quality and CCT of lighting has an impact on human comfort and productivity [21]–[23]. As a matter of fact, suitable visual lighting and color has been demonstrated to drastically reduce stress levels and even affect the mood of the occupants [24]. CCT control is generally achieved through the implementation of smart algorithms that optimize multi-color (typically RGB) LED light sources. Examples of these include work done by Gao et al. [25], Buso and Spiazzi [26], and Chen et al. [27]. Recently, Lee et al. presented a scheme for controlling the luminosity and CCT of a bi-color LED lamp by utilizing closed-loop control with feedback from a color sensor [28].

A notable gap in research is the direct control of the light spectrum, where the spectral power distribution (SPD) is precisely manipulated via control over a multi-channel LED lighting system. With this in mind, we developed a novel closed-loop smart algorithm to tune the SPD produced by a luminaire, based on feedback from a micro-spectrometer to offer increased tunability of the light output spectrum. A wireless multi-channel smart lighting system was also designed and implemented to verify the accuracy of the control algorithm. The smart algorithm and architectural framework of the system are described in this paper, along with the experimental outcomes. The rest of the paper is organized as follows: Section II describes the smart lighting system architecture; Section III presents our novel control algorithm; Section IV details the experimental results and discussion; and finally, Section V provides concluding remarks.

II. The Lighting System Architecture

The lighting system consists of a power supply module, wireless sensor module, micro-controller unit and the light engine. We use an ATMega328 8-bit AVR RISC-based micro-controller to modulate the duty cycle of the PWM signal that is sent to the dimming pins of the eight-channel LED driver. The micro-controller receives feedback from a wireless sensor module that is used by the smart control algorithm to shape the spectrum of the light output. The block diagram of the lighting system is shown in Fig. 1. In the following sub-sections, we describe the architecture of the light engine and the wireless sensor module.

A. The Light Engine

The light engine drives the generation of light for the smart luminaire, consisting of multiple LED channels and an LED driver. The goal of designing the light engine was to achieve a widely tunable light spectrum and to perform excellently as a general lighting source by providing high quality white light through color mixing. Whilst white light can be achieved with a simple RGB mix, utilizing extra primary emitters can increase the color rendering index (CRI) and CCT tunability, and therefore improve the light quality [26]. In order to achieve the aforementioned design goals, we chose a mix of eight LED channels with different peak wavelengths (listed in Table I); the LEDs were chosen based on previous research

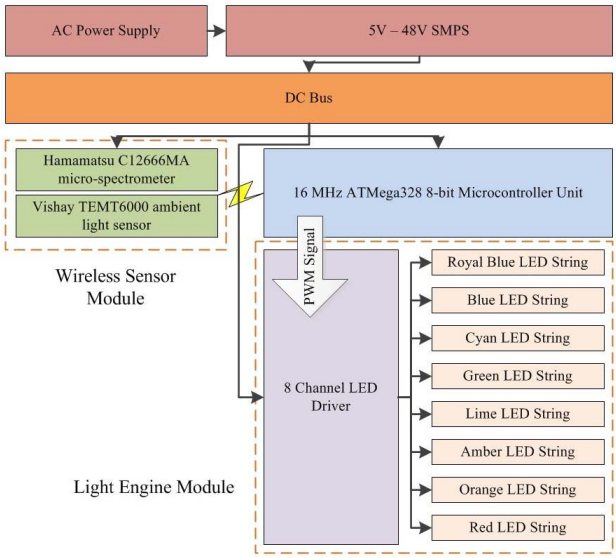

Fig. 1. The block diagram of the lighting system.

TABLE I
SUMMARY OF THE LEDS USED IN THE LIGHT ENGINE

LED Type	Color	Peak Wavelength (nm)	Maximum Luminous Flux (lm)	Number
CREE XBDROY	Royal Blue	447	53.6	3
CREE XBDBLU	Blue	467	220	4
Lumileds LXML-PE01	Cyan	504	536	5
CREE XBDGRN	Green	513	807	6
Lumileds LXML-PX02	Lime	542	1726	7
CREE XBDAMB	Amber	600	730	6
CREE XBDRDO	Red-Orange	623	490	3
CREE XBDRED	Red	634	490	4
		Total:	5053	38

that proposed a suitable mix of single color LEDs to achieve a white light of very high quality [29].

The number of LEDs for each channel were chosen for the light engine to achieve a producible CCT ranging from 2500K–8000K and a maximum light intensity of 5000 lumens. The radiant power of each channel required for this CCT range was used to determine the number of LEDs needed per channel. The LEDs are then arranged on a specially designed board, for which the distance between individual LEDs were calculated to achieve excellent color mixing. The measured SPDs of each LED channel are shown in Fig. 2(a). By modulating the intensities of individual LED channels, the spectral shape of the produced light and its CCT can be manipulated.

We also verified that the light engine can reproduce specific nominal CCTs accurately. A MacAdam ellipse is defined as a region on the chromaticity diagram where all colors bounded by this region are indistinguishable by the average human eye from the color at the center of the ellipse, and is the standard measure of a light's ability to faithfully reproduce specific CCTs [30]. We use the five-step $u'v'$ circle proposed by the CIE in 2014 to verify the ability of our light engine

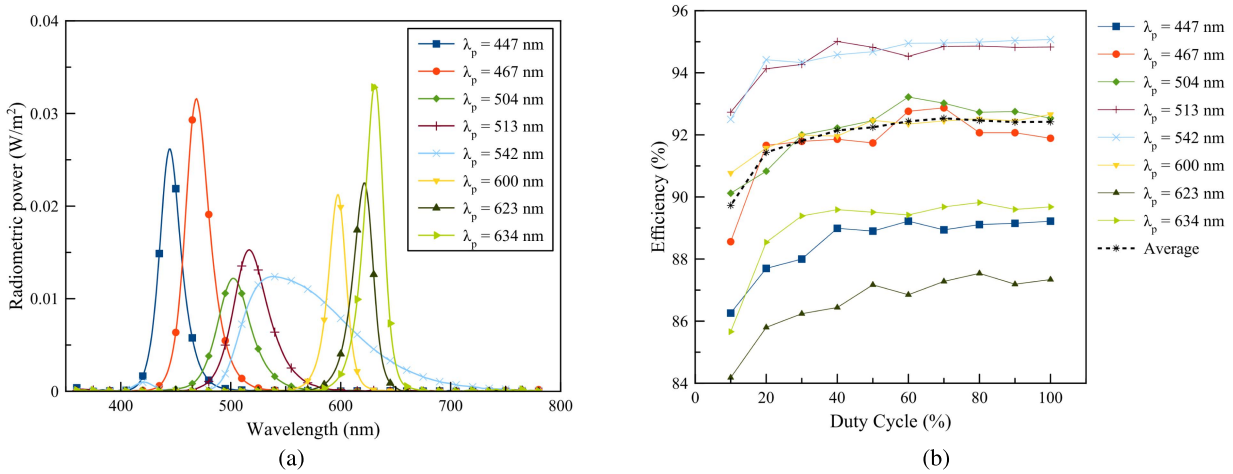

Fig. 2. The measured real-world performance of the light engine. (a) Light output spectral distribution. (b) Per-channel efficiency of the LED driver.

to reproduce specific CCTs accurately for the white region near the Planckian locus [31]. For a centre point (u'_c, v'_c), the five step $u'v'$ circle can be expressed by the equation:

$$(u' - u'_c)^2 + (v' - v'_c)^2 = (5.5 \times 10^{-3})^2 \quad (1)$$

The chromaticity difference between two color points can be expressed as the Euclidean distance between the points, which is the square root of Equation 1.

An eight-channel LED driver was designed to power the LEDs, using a LM3409 constant current buck converter [32] as the power controller. The buck converter contains a high side N-channel MOSFET switch with a suitable current limit. Each LED channel current can be modulated individually by a pulse width modulated (PWM) signal at a frequency of 1kHz per channel. Our designed driver is capable of supplying the maximum rated current of 700mA to each LED channel at the nominal input voltage of 30VDC. We measured the average electrical efficiency of the driver to be 91.96% using a power analyzer. Fig. 2(b) shows the measured per-channel efficiency of the LED driver.

Due to the close proximity of the LEDs and the high current needed to drive them, the light engine can generate large amounts of unwanted heat, especially at the higher light intensities. If heat is not removed efficiently, the LED peak wavelength may shift and the LEDs could have a shorter lifespan, or even fail entirely. Therefore, we mount the LEDs on a metal core printed circuit board (MCPCB) with a low thermal resistance of 150W/mK for a 1588μm plate. A heat sink with a thermal resistance of $1.2°C/W$ is also attached to the back of the circuit board to facilitate heat dispersion via convection.

B. The Wireless Sensor Module

The wireless sensor module contains a micro-spectrometer, a microcontroller and a ZigBee wireless module. The Hamamatsu C12666MA micro-spectrometer measures the spectrum of incident visible light (340nm - 780nm) with a maximum spectral resolution of 15nm or 256 pixels. The micro-spectrometer was calibrated according to the wavelength calibration coefficients provided by the manufacturer. The microcontroller reads the analog signals from the micro-spectrometer and converts them via an on-board ADC. We utilize the micro-spectrometer to provide feedback on the collective light spectrum shape and illuminance in a given space to the control system at a defined polling rate.

We considered common wireless protocols including the IEEE 802.15.4 ZigBee standard, the IEEE 802.11a/b/g/n/ac Wi-Fi standard and the IEEE 802.15.1 Bluetooth standard. The IEEE 802.15.4 ZigBee standard was chosen due to its low cost, low power consumption and low complexity [3]

Algorithm 1 Wireless Sensor Module Pseudocode

```
if millis() >= timeout then                    ▷ read at sampling period
    readSpectrometer();
    delay(10);                                 ▷ 10ms delay
    packet ← 1;
    timeout ← millis() + timeon;
end if
if packet ← 1 then
    payload[0] ← 1;                            ▷ synchronization bit
    payload[1] ← data[0] & 0xFF;
    payload[2] ← data[0] >> 8 & 0xFF;
    if saveSpectrum() ← 1 then                 ▷ save spectrum
        payload[3] ← 1;
    else
        payload[3] ← 0;
    end if
    xbee.send(tx);                             ▷ transmit packets
end if
for i ← 1, 256 do
    payload[0] ← 0;                            ▷ synchronization bit
    payload[1] ← data[i] & 0xFF;
    payload[2] ← data[i] >> 8 & 0xFF;
    payload[3] ← 0;
    xbee.send(tx);                             ▷ transmit packets
    delay(1);                                  ▷ 1ms delay
end for
```

Transmitted Packet									
Content	Frame Control	MSB	LSB	Identifier	Frame ID	Dest. Address	Options	Payload	Checksum
Size	1 byte	1 byte	1 byte	1 byte	1 byte	2 bytes	1 byte	19 bytes	1 byte

Payload										
Byte	**1**	**2**	**3**	**4**	**5**	**6**	**7**	**8**	**9**	**10**
Content	Lighting commands		Sync	Spec data[i]		Save	X		Y	
Byte	**11**	**12**	**13**	**14**	**15**	**16**	**17**	**18**	**19**	
Content	Z		V		CCT	Light data	Mode	u'	v'	

Fig. 3. Format of the transmited and received ZigBee packets.

which is suitable for intermittent transmission of sensor data. There are two transmission modes available with the 802.15.4 ZigBee standard, namely the transparent (AT) and the Packet (API) mode. We utilize the API mode with a PAN ID of 3335 and channel ID 0x0C to enable communication between a central coordinator and each wireless sensor module via packets. The advantage of the API mode is that it has a robust solution of dealing with dropped packets by sending and waiting for an acknowledgement (ACK) packet from the receiver to indicate a successful packet transmission. If the transmitter does not receive an ACK packet before the set timeout period, it will then resend the packet. The received packets also contain the address of the transmitting radios. The packet format is described in Fig. 3. Each transmitted packet contains 28 bytes, therefore 7168 bytes are required to transmit one spectrum. The transmission of each spectrum completes in around 300 ms, with a preset 1 ms delay in between the transmission of each discrete vector value.

The payload includes spectral data, color coordinates, CCT, ambient light data, and lighting commands, where the lighting commands and mode bytes are used for manual channel intensity control or to enable/disable other automatic control modes. The spectral data is an array of 256 integer values with a size of 16 bits per packet. The synchronization byte is the third byte of the payload and is used to point to the start of the data string to ensure that the data is transmitted and received in the correct order. The size of data to be transmitted is 16 bits or 2 bytes for each data type. Therefore, each message is broken into 2 parts (high and low byte) to be transmitted and then reassembled at the receiver. The low byte is shifted 8 bits to the right while the high byte is ANDed with 16 bits of 1s. The receiver reverses this to obtain the original transmitted data as described in Algorithm 1.

III. The Control Algorithm

In order to control the light spectrum in a room, we start with a pre-defined target spectrum. The target spectrum can be read wirelessly via the spectral sensor or defined by the user with a 15nm spectral resolution (which matches the resolution of the spectral sensor). The micro-controller reads the instantaneous ambient light spectrum in the room by gathering light spectral feedback from the wireless sensor module at a defined polling rate. The instantaneous ambient light spectrum

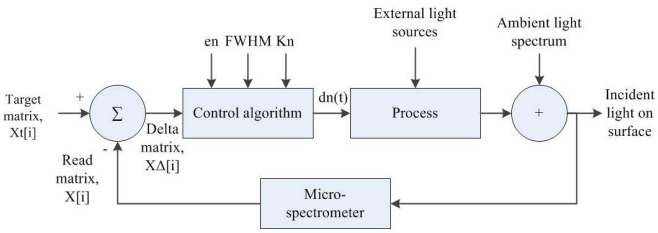

Fig. 4. The closed-loop control system.

is continuously compared with the target spectrum and repeatedly tuned to converge towards the target spectrum within a $\Delta u'v'$ tolerance of 5.5×10^{-3} (five-step $u'v'$ unit circle) by defining the driving current in each LED channel. The control algorithm (Fig. 4) determines the pulse width modulated (PWM) signal that is sent to the LED driver controlling each channel. By varying the duty cycle, $d_n(t)$ of the PWM signal, the micro-controller can regulate the driving current, and as a result, the light intensity of each LED channel. The micro-controller writes the duty cycle as an unsigned 8 bit integer (0-255). The control variables used in this control system are summarized in Table II.

Two stopping criteria are implemented for this control system to achieve accurate spectral shape reproduction and chromaticity replication. To achieve that, the goals of the control algorithm are to minimize the total difference between the instantaneous light spectrum and the target spectrum until it falls within an acceptable range of errors, and to continuously tune the output spectrum until the Euclidean distance, $\Delta u'v'$ between the target and tuned spectrum is less than the acceptable $\Delta u'v'$ of 5.5×10^{-3}.

The block diagram of the closed-loop control system is shown in Fig. 4. The target spectrum is a vector of 256 values (8 bits) with a spectral resolution of 15nm for the micro-spectrometer and is saved as a vector of values in the micro-controller EEPROM memory, which can be represented with the following equation:

$$X_t[i] = [X_{t0}, X_{t1}, \ldots, X_{ti-2}, X_{ti-1}] \tag{2}$$

The instantaneous ambient light spectrum read by the micro-spectrometer is stored in a separate vector

TABLE II
DESCRIPTION OF THE CONTROLLER VARIABLES

Variable	Description
i	Number of discrete spectral data values
$X_t[i]$	Target spectrum vector
$X[i]$	Instantaneous spectrum vector
$\hat{X_t}[i]$	Normalized target spectrum vector
$\hat{X}[i]$	Normalized instantaneous spectrum vector
$X_\Delta[i]$	Delta vector
$FWHM_n$	Channel full width half maximum
$\hat{X_{\Delta n}}[i]$	Error vector of each channel
$S_n(t)$	Sum of $\hat{X_{\Delta n}}[i]$ data
$d_n(t)$	PWM duty cycle signal
K_n	Adjusted step size of the duty cycle
e_n	Acceptable error margin

defined as:

$$X[i] = [X_0, X_1, \ldots, X_{i-2}, X_{i-1}] \tag{3}$$

The vectors, $X_t[i]$ and $X[i]$ records the A/D counts of each discrete specified wavelength from 340nm - 780nm. The maximum and minimum of both vectors are obtained through a bubble sorting algorithm and are denoted as max and min. These vectors are then normalized. where $\hat{X}_t[i]$ and $\hat{X}[i]$ are defined as:

$$\hat{X}_t[i] = \frac{X_t[i] - min}{max - min} = [\frac{X_{t0} - min}{max - min}, \frac{X_{t1} - min}{max - min}, \ldots, \frac{X_{ti-2} - min}{max - min}, \frac{X_{ti-1} - min}{max - min}] \tag{4}$$

$$\hat{X}[i] = \frac{X[i] - min}{max - min} = [\frac{X_0 - min}{max - min}, \frac{X_1 - min}{max - min}, \ldots, \frac{X_{i-2} - min}{max - min}, \frac{X_{i-1} - min}{max - min}] \tag{5}$$

The difference between the instantaneous vector and the target vector is calculated and defined as $X_\Delta[i]$, representing the error magnitude for discrete wavelengths. A positive value indicates that the intensity of that particular wavelength needs to be increased while a negative value indicates that it needs to be decreased.

$$X_\Delta[i] = \hat{X}_t[i] - \hat{X}[i] = [\hat{X}_{t0} - \hat{X_0}, \hat{X}_{t1} - \hat{X_1}, \ldots, \hat{X}_{ti-2} - \hat{X}_{i-2}, \hat{X}_{ti-1} - \hat{X}_{i-1}] \tag{6}$$

Since there are eight LED channels, the control system has eight control points. Therefore, $X_\Delta[i]$ is further broken down into eight vectors corresponding to the eight control points which are centered around the peak wavelengths of each channel and have a roll-off length defined by the full width half maximums (FWHM) of each individual LED channel, $FWHM_n$. The variable n is the n^{th} value within $X_\Delta[i]$ (0-255) corresponding to each peak wavelength as read by the micro-controller. This data is obtained experimentally for each LED channel and is shown as follows:

$$n = \begin{cases} 57, & \text{royal blue } (\lambda_p : 447nm) \\ 66, & \text{blue } (\lambda_p : 467nm) \\ 83, & \text{cyan } (\lambda_p : 504nm) \\ 88, & \text{green } (\lambda_p : 513nm) \\ 101, & \text{lime } (\lambda_p : 542nm) \\ 130, & \text{amber } (\lambda_p : 600nm) \\ 142, & \text{orange } (\lambda_p : 623nm) \\ 147, & \text{red } (\lambda_p : 634nm) \end{cases} \tag{7}$$

A vector $X_{\Delta n}[FWHM_n]$ is defined to contain the discrete wavelength errors of each channel that needs to be corrected by the control algorithm. There are a total of eight $X_{\Delta n}[FWHM_n]$ vectors which are defined by:

$$X_{\Delta n}[FWHM_n] = [X_{\Delta n - FWHM_n/2}, X_{\Delta n+1-FWHM_n/2}, \ldots, X_{\Delta n-1+FWHM_n/2}, X_{\Delta n+FWHM_n/2}] \tag{8}$$

To obtain the total magnitude of the channel error, the sum of each delta vector $S_n(t)$ is calculated, where n represents the LED channel, as defined in Equation 7. The larger the channel error magnitude, the further the control point is from the target spectrum. A positive value indicates that the channel intensity needs to be increased and vice-versa for a negative value.

$$S_n(t) = \sum_{0}^{FWHM_n} X_{\Delta n}[FWHM_n] \tag{9}$$

The goals of the control algorithm are to minimize the sum $S_n(t)$ until it falls within the user-defined acceptable range of errors, e_n and to continuously tune the output spectrum until the Euclidean distance, $\Delta u'v'$ between the target and tuned spectrum is less than the acceptable $\Delta u'v'$ of 5.5×10^{-3}. To achieve this, the duty cycle, $d_n(t)$ of the PWM signal, $p(t)$ for each channel is modulated depending on the value of $S_n(t)$ as defined by:

$$d_n(t) = \begin{cases} d_n(t) - K_n & \text{if } S_n(t) > e_n \\ d_n(t) + K_n & \text{if } S_n(t) < -e_n \end{cases} \tag{10}$$

The user-defined error variable, e_n sets the maximum and minimum threshold of the range within which the system achieves its steady state. The magnitude of the sum of each delta vector, $|S_n(t)|$ is minimized by adding or subtracting an amount determined by the gain, K_n until it falls within the aforementioned acceptable error range. The gain is tuned using adaptive gain tuning to increase the response time and accuracy of the control system, whereby it is increased when the error is large and decreased as the control point converges towards the target spectrum as described below:

$$K_n = \begin{cases} 20 & \text{if } |S_n(t)| > 3FWHM_n|e_n| \\ 10 & \text{if } |e_n| + FWHM_n < |S_n(t)| \ldots, \\ & \quad \leq |e_n| + 2FWHM_n \\ 5 & \text{if } |e_n| < |S_n(t)| \leq |e_n| + FWHM_n \end{cases} \tag{11}$$

This is repeated for all eight channels in real time. If the calculated error sum $S_n(t)$ falls within the acceptable error margin e_n, the control system does not react. A larger e_n

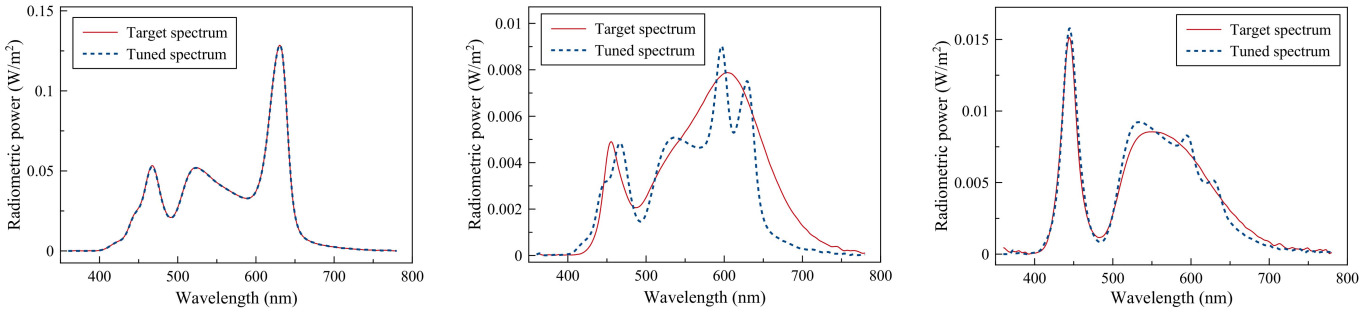

Fig. 5. Comparison between the original and tuned spectra for various light sources. (a) Light engine. (b) Warm white LED. (c) Cool white LED.

TABLE III
COMPARISON BETWEEN THE ORIGINAL AND TUNED SPECTRA OF VARIOUS LIGHT SOURCES

Parameter	Light Engine		Warm White LED		Cool White LED	
	Target Spectrum	Tuned Spectrum	Target Spectrum	Tuned Spectrum	Target Spectrum	Tuned Spectrum
x	0.3978	0.3987	0.4218	0.4261	0.3306	0.3237
y	0.3762	0.3769	0.3954	0.3994	0.3452	0.3470
u'	0.2368	0.2371	0.2445	0.2458	0.2040	0.1987
v'	0.5039	0.5044	0.5157	0.5179	0.4794	0.4793
T	3547K	3532K	3198K	3151K	5587K	5895K
CRI	78	78	83	80	70	70
δ_{uv}	-0.0049	-0.0048	-0.0012	-0.0003	0.003	0.007
$\Delta u'v'$	5.83×10^{-4}		2.50×10^{-3}		5.30×10^{-3}	
Δ_{CCT}	0.42 %		1.47 %		5.22 %	

will increase the stability of the system but may decrease its accuracy if too large. The sum of errors for each discrete control point is minimized over time until it reaches steady state. The gain, acceptable error range, and channel vector size can be further tuned to increase the control system response time and accuracy. When the sum, $S_n(t)$ of all eight control points fall within the acceptable margin of errors, e_n, the produced light spectrum will have fully converged towards the target light spectrum, subject to the light engine capability.

The Euclidean distance between the target and tuned spectrum is continuously calculated. The control system is only deemed to reach steady state when the Euclidean distance between the two spectra is less than 5.5×10^{-3}, placing the chromaticity coordinates of the tuned spectrum within a five-step $u'v'$ unit circle distance from the target spectrum chromaticity coordinates.

IV. EXPERIMENTAL RESULTS AND DISCUSSION

A. Experimental Setup

We deployed the lighting system in a room designed to replicate a standard living room with large windows, carpeted floor, white walls, and a ceiling height of 2.4 m. The test setup simulates a common lighting scene with external disturbances (ambient daylight) where the lighting system was mounted as a lighting fixture with an attached optical diffuser on the ceiling. We placed the wireless sensor module at table height to allow it to provide accurate spectral data feedback to the lighting system.

Using this experimental setup, various tests were conducted to assess the ability and accuracy of our control system to replicate different light sources (light engine, warm white LED, and cool white LED). The spectral data of the target spectrum was saved into the micro-controller EEPROM memory via the wireless sensor module. Then, the duty cycles of all channels were set to zero and the control system allowed to tune the light output SPD towards the saved target SPD until it reached steady state as defined by our control algorithm. Once steady state was achieved, we measured the chromaticity coordinates (x, y, u', v'), δ_{uv}, color rendering index (CRI), and correlated color temperature (CCT) using a factory-calibrated Konica Minolta CL-500A illuminance spectrophotometer. Based on the measured values, the Euclidean distance, $\Delta u'v'$ between the spectra was then calculated. The results of the tests are reported in the following subsections.

B. Light Engine Light Source

The first target spectrum was a light spectrum produced using the light engine, where multiple LED channels were set to varying intensities. The SPD of the tuned spectrum compared to the target spectrum upon reaching steady state is shown in Fig. 5(a), while the measured results are listed in Table III. From the results, it is obvious that the tuned spectrum is very similar to the target spectrum, with a CCT difference of only 0.42% and an Euclidean distance that falls well within a five-step $u'v'$ circle. The CRI and δ_{uv} are also maintained. This result validates the accuracy of the control system in reproducing spectra with similar peak wavelengths as the light engine.

C. Warm White LED Light Source

Next, phosphor-converted CREE XT-E warm white LEDs were used to produce the target spectrum. The target spectrum has two discrete peaks at 455 nm and 600 nm, which are different than the peak wavelengths of the LEDs in the light engine. The SPD of the tuned spectrum compared to the target spectrum upon reaching steady state is shown in Fig. 5(b), while the measured results are listed in Table III. Upon first inspection, it is noticeable that the tuned spectrum follows the general shape of the target spectrum with amplitude differences at certain wavelengths. This shows that it is not possible for the light engine to replicate this target spectrum fully due to the limited number of channels in the light engine. Theoretically, full replication can be achieved with an increased number of primary emitters, notably with similar peak wavelengths as the target spectrum. However, the measured color coordinates are very close, with an Euclidean distance of only 2.5×10^{-3} between the target and tuned spectra. Also, the CRI, δ_{uv} and CCT are maintained. Therefore, we can conclude that the tuned spectrum is an adequate replacement for the target spectrum.

D. Cool White LED Light Source

The same experiment was repeated using phosphor-converted CREE XT-E cool white LEDs to produce the target spectrum. The target spectrum has two discrete peaks at 447 nm and 555 nm. Interestingly, the 447 nm peak is similar to the peak wavelength of one of the light engine primary emitters. The SPD of the tuned spectrum compared to the target spectrum upon reaching steady state is shown in Fig. 5(c), while the measured results are listed in Table III. Looking at the graph, we notice that the tuned spectrum follows the general shape of the target spectrum, with a perfectly matched blue peak at 447 nm while the broader, phosphor-converted peak is matched by the utilization of multiple primary emitters over that particular wavelength range. Here, the spectrum is more closely matched compared to the warm white LED light source as the target spectrum matches the selected primary emitters more closely.

The measured color coordinates are very similar, with an Euclidean distance of 5.3×10^{-3}. The CRI, δ_{uv} and CCT are also maintained. Therefore, we can conclude that the tuned spectrum is an adequate replacement for the target spectrum.

E. Replication Time

The time taken for the control system to reach steady state represents the time required for the smart luminaire to fully replicate a target spectrum. In this case, faster is not always better, as a longer replication time provides a more gradual change which may be more comfortable, whilst a short replication time will result in an abrupt change in the perceived color of the light output, which can be very jarring. On the other hand, the tuning period should not be too long, as a longer tuning period increases the time that the room light spectrum is in transition and also places a heavier strain on the micro-controller which in turn increases the power consumption of the smart luminaire and wireless sensor module.

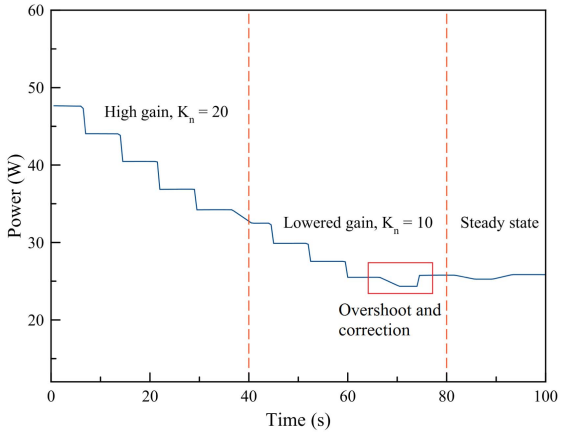

Fig. 6. The power consumption of the control system as it achieves steady state over the tuning period. The gain amplitude is adapted depending on how close the channel is to achieving its steady state.

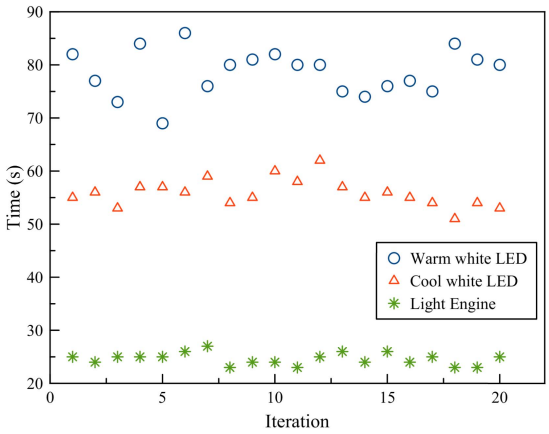

Fig. 7. The time taken for the control system to reach steady state for 20 trials with a polling rate of 5 seconds.

Fig. 6 illustrates the response of the control system as it converges towards its steady state to replicate a target spectrum. The power consumption of the luminaire is inherently tied to the intensity of the LED channels. The rate of change of the power consumption is therefore suitable to represent the rate of change of the control system as it works towards reaching steady state. The rate of change is increased when the gain is high, and lowered when the gain is lowered as defined in the control algorithm.

The replication time is highly dependent on the polling rate of the wireless sensor module as the control algorithm needs to read the instantaneous ambient spectral data to tune the light spectrum. To experiment on the replication time for different spectra, we repeatedly tuned the output light spectrum to converge towards the light spectra of the aforementioned light engine, warm white LED, and cool white LED sources for a total of 20 iterations each at a polling rate of 5 seconds. The results are shown in Fig. 7. Interestingly, we notice that the replication time of the spectrum produced by the light engine is the shortest, followed by the spectrum of a cool white LED, while the replication time of a warm white LED spectrum is the longest. We believe this shows that the replication time

decreases as the peak wavelengths of the target spectrum are more closely matched with the selected primary emitters. If the peak wavelengths are not closely matched, the number of channels that need to be tuned to compensate increases, thus increasing the tuning period. Similarly, broader target spectra should also increase the required tuning period.

V. Conclusion

In this paper, we described the design and implementation of a tunable smart lighting system with eight LED channels incorporating a novel closed-loop control algorithm to tune the light output towards target spectra. The framework of the smart lighting system, including the LED channels, LED driver, IEEE 802.15.4 ZigBee wireless connectivity, and micro-controller was also outlined.

The performance of the control algorithm was validated experimentally using three different light sources to replicate the target light spectrum. We found that the SPD of the tuned spectrum closely matches that of the target spectrum if the peak wavelengths are similar, as shown by the results of replicating a target spectrum produced by the light engine. If the peak wavelengths of the primary emitters differ from the target spectrum, the control system compensates by utilizing multiple primary emitters over that particular wavelength instead. This leads to some differences in the spectral shape. However, we found that important metrics such as the color coordinates, CCT, CRI, and δ_{uv} are maintained. Experimentally, an accuracy of 1.47% and 5.22% for the CCTs were achieved, with Euclidean distances, $\Delta u'v'$ between the target and tuned light spectra of 2.5×10^{-3} and 5.3×10^{-3} for a warm white LED and a cool white LED light spectrum respectively.

References

[1] M. Magno, T. Polonelli, L. Benini, and E. Popovici, "A low cost, highly scalable wireless sensor network solution to achieve smart LED light control for green buildings," *IEEE Sensors J.*, vol. 15, no. 5, pp. 2963–2973, May 2015.

[2] G. Dhivya, K. Subaashini, J. Shamshudeen, G. Rekha, and R. Pitchiah, "Wirelessly controlled LED fixture with heat sink–Design and implementation," in *Proc. IEEE Int. Conf. Consum. Electron. (ICCE)*, Las Vegas, NV, USA, Jan. 2013, pp. 506–507.

[3] Y. Liu and R. Sahandi, "Zigbee network for remote patient monitoring on general hospital wards," in *Proc. 22 Int. Symp. Inf., Commun. Autom. Technol. (ICAT)*. Sarajevo, Bosnia and Herzegovina, Oct. 2009, pp. 1–7.

[4] F. Leccese, "Remote-control system of high efficiency and intelligent street lighting using a ZigBee network of devices and sensors," *IEEE Trans. Power Del.*, vol. 28, no. 1, pp. 21–28, Jan. 2013.

[5] L. Hardy and M. Gafen, "A synchronized wireless mesh network model for intelligent lighting control: Case study," in *Proc. 7th Int. Conf. Netw. Sens. Syst. (INSS)*, Kassel, Germany, Jun. 2010, pp. 153–156.

[6] L. Lian and L. Li, "Wireless dimming system for LED street lamp based on ZigBee and GPRS," in *Proc. 3rd Int. Conf. Syst. Sci., Eng. Design Manuf. Inf. (ICSEM)*, Chengdu, China, Oct. 2012, pp. 100–102.

[7] Y. K. Tan, T. P. Huynh, and Z. Wang, "Smart personal sensor network control for energy saving in DC grid powered LED lighting system," *IEEE Trans. Smart Grid*, vol. 4, no. 2, pp. 669–676, Jun. 2013.

[8] J. Byun, B. Jeon, J. Noh, Y. Kim, and S. Park, "An intelligent self-adjusting sensor for smart home services based on ZigBee communications," *IEEE Trans. Consum. Electron.*, vol. 58, no. 3, pp. 794–802, Aug. 2012.

[9] K. Gill, S.-H. Yang, F. Yao, and X. Lu, "A ZigBee-based home automation system," *IEEE Trans. Consum. Electron.*, vol. 55, no. 2, pp. 422–430, May 2009.

[10] D.-M. Han and J.-H. Lim, "Smart home energy management system using IEEE 802.15.4 and ZigBee," *IEEE Trans. Consum. Electron.*, vol. 56, no. 3, pp. 1403–1410, Aug. 2010.

[11] A. Pandharipande, D. Caicedo, and X. Wang, "Sensor-driven wireless lighting control: System solutions and services for intelligent buildings," *IEEE Sensors J.*, vol. 14, no. 12, pp. 4207–4215, Dec. 2014.

[12] S.-R. Lim, D. Kang, O. A. Ogunseitan, and J. M. Schoenung, "Potential environmental impacts of light-emitting diodes (LEDs): Metallic resources, toxicity, and hazardous waste classification," *Environ. Sci. Technol.*, vol. 45, no. 1, pp. 320–327, 2010.

[13] A. Fernandez-Montes, L. Gonzalez-Abril, J. A. Ortega, and F. V. Morente, "A study on saving energy in artificial lighting by making smart use of wireless sensor networks and actuators," *IEEE Netw.*, vol. 23, no. 6, pp. 16–20, Nov. 2009.

[14] S. Matta and S. M. Mahmud, "An intelligent light control system for power saving," in *Proc. 36th Annu. Conf. IEEE Ind. Electron. Soc. (IECON)*, Nov. 2010, pp. 3316–3321.

[15] E. Juntunen *et al.*, "A smart LED luminaire for energy savings in pedestrian road lighting," *Lighting Res. Technol.*, vol. 47, no. 1, pp. 103–115, 2015.

[16] D. Park, Z. Liu, and H. Lee, "A 40 V 10 W 93%-efficiency current-accuracy-enhanced dimmable LED driver with adaptive timing difference compensation for solid-state lighting applications," *IEEE J. Solid-State Circuits*, vol. 49, no. 8, pp. 1848–1860, Aug. 2014.

[17] S. Wang, X. Ruan, K. Yao, S.-C. Tan, Y. Yang, and Z. Ye, "A flicker-free electrolytic capacitor-less ac–dc LED driver," *IEEE Trans. Power Electron.*, vol. 27, no. 11, pp. 4540–4548, Nov. 2012.

[18] B. V. Neida, D. Manicria, and A. Tweed, "An analysis of the energy and cost savings potential of occupancy sensors for commercial lighting systems," *J. Illuminating Eng. Soc.*, vol. 30, no. 2, pp. 111–125, 2001.

[19] J. Byun, I. Hong, B. Lee, and S. Park, "Intelligent household LED lighting system considering energy efficiency and user satisfaction," *IEEE Trans. Consum. Electron.*, vol. 59, no. 1, pp. 70–76, Feb. 2013.

[20] J. Higuera, W. Hertog, M. Perálvarez, J. Polo, and J. Carreras, "Smart lighting system ISO/IEC/IEEE 21451 compatible," *IEEE Sensors J.*, vol. 15, no. 5, pp. 2595–2602, May 2015.

[21] J. Veitch, G. Newsham, P. Boyce, and C. Jones, "Lighting appraisal, well-being and performance in open-plan offices: A linked mechanisms approach," *Lighting Res. Technol.*, vol. 40, no. 2, pp. 133–151, 2008.

[22] S. A. Fotios, "Lamp colour properties and apparent brightness: A review," *Lighting Res. Technol.*, vol. 33, no. 3, pp. 163–178, 2001.

[23] D. H. W. Li and J. C. Lam, "Evaluation of lighting performance in office buildings with daylighting controls," *Energy Buildings*, vol. 33, no. 8, pp. 793–803, Oct. 2001.

[24] H. Dalke *et al.*, "Colour and lighting in hospital design," *Opt. Laser Technol.*, vol. 38, nos. 4–6, pp. 343–365, Jun./Sep. 2006.

[25] Y. Gao, H. Wu, J. Dong, and G. Q. Zhang, "Constrained optimization of multi-color LED light sources for color temperature control," in *Proc. 12th China Int. Forum Solid State Lighting (SSLCHINA)*, Nov. 2015, pp. 102–105.

[26] S. Buso and G. Spiazzi, "White light solid state lamp with luminance and color temperature control," in *Proc. Brazilian Power Electron. Conf. (COBEP)*, Natal, Brazil, Sep. 2011, pp. 837–843.

[27] H.-T. Chen, S.-C. Tan, and S. Y. Hui, "Nonlinear dimming and correlated color temperature control of bicolor white LED systems," *IEEE Trans. Power Electron.*, vol. 30, no. 12, pp. 6934–6947, Dec. 2015.

[28] A. T. L. Lee, H. Chen, S.-C. Tan, and S. Y. Hui, "Precise dimming and color control of LED systems based on color mixing," *IEEE Trans. Power Electron.*, vol. 31, no. 1, pp. 65–80, Jan. 2016.

[29] S. Linke, R. Hegel, O. Esser, and A. Mahlkow, "Simulating of led sum-spectra for best color rendering index along the black body curve—A reverse engineering attempt," in *Proc. CIE, Lighting Quality Energy Efficiency*, Kuala Lumpur, Malaysia, Apr. 2014.

[30] G. Wyszecki and W. S. Stiles, *Color Science*, vol. 8. New York, NY, USA: Wiley, 1982.

[31] Y. Ohno and P. Blattner, "Chromaticity difference specification for light sources," Int. Commiss. Illumination, Tech. Rep. CIE TN 001, 2014.

[32] *LM3409xx/Q1 PFET Buck Controller for High-Power LED Drivers*, snvs602k ed., Texas Instrum., Dallas, TX, USA, Jul. 2015.

Ivan Chew, photograph and biography not available at the time of publication.

Vineetha Kalavally, photograph and biography not available at the time of publication.

Chee Pin Tan, photograph and biography not available at the time of publication.

Jussi Parkkinen, photograph and biography not available at the time of publication.